doi:10.1016/j.jmb.2003.09.014 J. Mol. Biol. (2004) 336, 1211–1221

JMB

Available online at www.sciencedirect.com

SCIENCE DIRECT®

ELSEVIER

NMR Structure of the Integral Membrane Protein OmpX

César Fernández, Christian Hilty, Gerhard Wider*, Peter Güntert and Kurt Wüthrich

Institut für Molekularbiologie und Biophysik, Eidgenössische Technische Hochschule Zürich CH-8093 Zürich, Switzerland

*Corresponding author

The structure of the integral membrane protein OmpX from *Escherichia coli* reconstituted in 60 kDa DHPC micelles (OmpX/DHPC) was calculated from 526 NOE upper limit distance constraints. The structure determination was based on complete sequence-specific assignments for the amide protons and the Val, Leu, and Ile(δ^1) methyl groups in OmpX, which were selectively protonated on a perdeuterated background. The solution structure of OmpX in the DHPC micelles consists of a well-defined, eight-stranded antiparallel β-barrel, with successive pairs of β-strands connected by mobile loops. Several long-range NOEs observed outside of the transmembrane barrel characterize an extension of a four-stranded β-sheet beyond the height of the barrel. This protruding β-sheet is believed to be involved in intermolecular interactions responsible for the biological functions of OmpX. The present approach for *de novo* structure determination should be quite widely applicable to membrane proteins reconstituted in mixed micelles with overall molecular masses up to about 100 kDa, and may also provide a platform for additional functional studies.

Keywords: TROSY; protein structure; OmpX; membrane proteins; micelles

Introduction

Membrane proteins constitute about one third of all proteins in living organisms. However, presently only about 50 entries in the Protein Data Bank (PDB)[1] represent three-dimensional (3D) structures of integral membrane proteins. This contrasts with more than 19,000 PDB entries of soluble proteins. In the ongoing structural genomics projects, membrane protein structure determination thus remains a challenge. Encouragingly, significant progress has recently been made in the areas of high-yield expression, purification and refolding of membrane proteins,[2–4] and important methodological advances have been achieved in the field of membrane protein structure determination by X-ray crystallography and NMR spectroscopy. As a result, about half of the membrane protein structures in the PDB have been deposited within the last two years. Knowledge of 3D structures of this class of proteins is fundamental to the understanding of a wide spectrum of biological functions, and to the development of new drugs that target membrane proteins.

For studies with solution NMR, the size of the mixed protein–detergent micelles needed to solubilize membrane proteins in water is beyond the limits of conventional NMR experiments, which would yield spectra with poor resolution and low signal-to-noise ratio. The use of the principles of transverse relaxation-optimized spectroscopy (TROSY)[5] at high magnetic fields, combined with refined isotope labeling strategies[6] now extends NMR studies to structures with molecular masses above 100 kDa.[7–9] Recent results include obtaining backbone resonance assignments and the three-dimensional folds of the *E. coli* outer membrane proteins OmpX,[10,11] OmpA[11–13] and PagP,[14] and physicochemical studies on other

Present addresses: C. Fernández, Novartis Pharma AG, P.O. Box, 4002 Basel, Switzerland; P. Güntert, RIKEN Genomic Sciences Center, 1-7-22 Suehiro, Tsurumi, Yokohama 230-0045, Japan.

Abbreviations used: 3D, three-dimensional; DHPC, dihexanoylphosphatidylcholine (1,2-dihexanoyl-*sn*-glycero-3-phosphocholine); NOE, nuclear Overhauser effect; NOESY, NOE spectroscopy; OmpX, outer membrane protein X from *Escherichia coli*; PDB, Protein Data Bank; ppm, parts per million; RMSD, root-mean-square distance; TROSY, transverse relaxation-optimized spectroscopy.

E-mail address of the corresponding author: gsw@mol.biol.ethz.ch

integral membrane proteins in micellar environments.[15–17]

The 148-residue outer membrane protein X (OmpX) from *E. coli*, for which the crystal structure in the presence of the detergent *n*-octyltetraoxyethylene is known,[18] has been used in our laboratory as a model system for the development of NMR techniques for membrane protein structure determination and for folding studies. Here, the previous backbone resonance assignments obtained using uniformly ^{2}H,^{13}C,^{15}N-labeled OmpX[10,11] are supplemented by data collection with a perdeuterated OmpX sample with selectively protonated Val, Leu, and Ile(δ^1) methyl groups, [u-^{2}H,^{13}C,^{15}N/L,V,Iδ^1-$^{13}CH_3$]-OmpX.[19,20] The additional nuclear Overhauser effects (NOEs) from methyl groups to other methyl groups and to amide protons resulted in a complete structure determination of OmpX in DHPC micelles, which is supplemented with data on the dynamics and on conformational equilibria of OmpX/DHPC based on measurements of heteronuclear $^{15}N\{^{1}H\}$-NOEs and backbone amide proton exchange rates.

Results

Collection of conformational constraints and structure calculation

The collection of conformational constraints was based on complete sequence-specific assignments for the backbone resonances,[10] and the Val, Leu, and Ile(δ^1) methyl groups.[20] Figure 1 shows [ω_1(^{1}H), ω_3(^{1}H)]-strips taken from 3D ^{15}N-resolved [^{1}H,^{1}H]-NOESY and 3D ^{13}C-resolved [^{1}H,^{1}H]-NOESY spectra of [u-^{2}H,^{13}C,^{15}N/L,V,Iδ^1-$^{13}CH_3$]-OmpX/DHPC recorded with a mixing time of 200 ms, where the labels identify cross-peaks corresponding to long-range or medium-range NOEs. It is readily apparent that these include a large number of NOEs involving Val, Leu, and Ile(δ^1) methyl groups. The resulting input for the CYANA structure calculation[21] contained 526 unambiguously assigned, meaningful NOE upper limit distance constraints, of which 255 were long-range NOEs. Using these experimental data, two structures were calculated (Figure 2). The first one was derived from "data set I", containing the NOE upper distance constraints, and dihedral angle constraints obtained from the ^{13}C chemical shifts (Figure 2(A)). The second structure was obtained from the same data supplemented with 68 upper limit and 68 lower limit distance constraints to account for 34 hydrogen bonds (data set II, Figure 2(B)). These hydrogen bonds were identified automatically by CYANA in the bundle of conformers obtained from data set I (see Materials and Methods for details). All the amide protons involved in the thus identified hydrogen bonds showed slowed exchange with the solvent (Figures 3(D) and 4(B)).

There are only few, quite small residual constraint violations (Table 1), which shows that the input data represent a self-consistent set, and that the constraints are well satisfied in the calculated conformers. This is true for both data sets I and II, showing that the 34 automatically determined hydrogen bonds are fully consistent with the NOE data. For the data set I, the RMSD values relative to the mean coordinates for the backbone atoms are 1.13 Å in the best-defined region of the β-barrel (see Table 1), and 1.42 Å for all residues located in the regular secondary structure elements. The corresponding numbers for the structure calculated with automatically determined hydrogen bond constraints (data set II) were 0.93 Å and 1.17 Å, respectively.

NMR solution structure of OmpX/DHPC

The solution structure of OmpX in DHPC micelles consists of an eight-stranded antiparallel β-barrel, with the individual strands containing the residues 3–13 (β1), 21–31 (β2), 38–50 (β3), 58–71 (β4), 78–93 (β5), 99–117 (β6), 122–131 (β7) and 136–146 (β8) (Figure 2(A)–(C)). Successive pairs of β-strands are connected by extracellular loops containing the residues 14–20 (L1), 51–57 (L2), 94–98 (L3) and 132–135 (L4), and by periplasmic turns consisting of the residues 32–37 (T1), 72–77 (T2) and 118–121 (T3) (same nomenclature as Vogt & Schulz[18]). As a peculiar feature of OmpX, the two extracellular loops L2 and L3 (Figure 2(C)) form a regular four-stranded sheet, which contains part of the strands β3, β4, β5 and β6 and extends beyond the confines of the barrel as a "protruding flag". The core of the barrel is well defined, whereas the solvent-exposed, protruding part of the β-structure is significantly less well ordered. The same holds for the loops and turns, with outstandingly large disorder for the loops L2 and L3 at the end of the protruding β-sheet (Figures 2(A) and (B), and 3(B)).

Conformational equilibria and dynamics of OmpX in DHPC micelles

This section supplements the determination of the molecular geometry (Figure 2(C)) with data on the local precision of the structure determination, amide proton exchange studies, and measurements of spin relaxation parameters.

The plots of the global backbone displacements[22] *versus* the sequence (Figure 3(B)) show that all β-strands within the barrel are well defined. Increased conformational disorder is observed for the polypeptide segments 15–22 (including L1), 32–37 (including T1), 50–60 (including L2), 73–78 (including T2), 90–103 (including L3), 117–120 (including T3) and 133–135 (including L4), i.e. all loop regions and adjacent residues. The segments with the lowest displacements (Figure 3(B)) coincide well with the regions with high density of NOE distance constraints (Figure 3(A)). Nearly all NOEs to the selectively methyl-protonated Val,

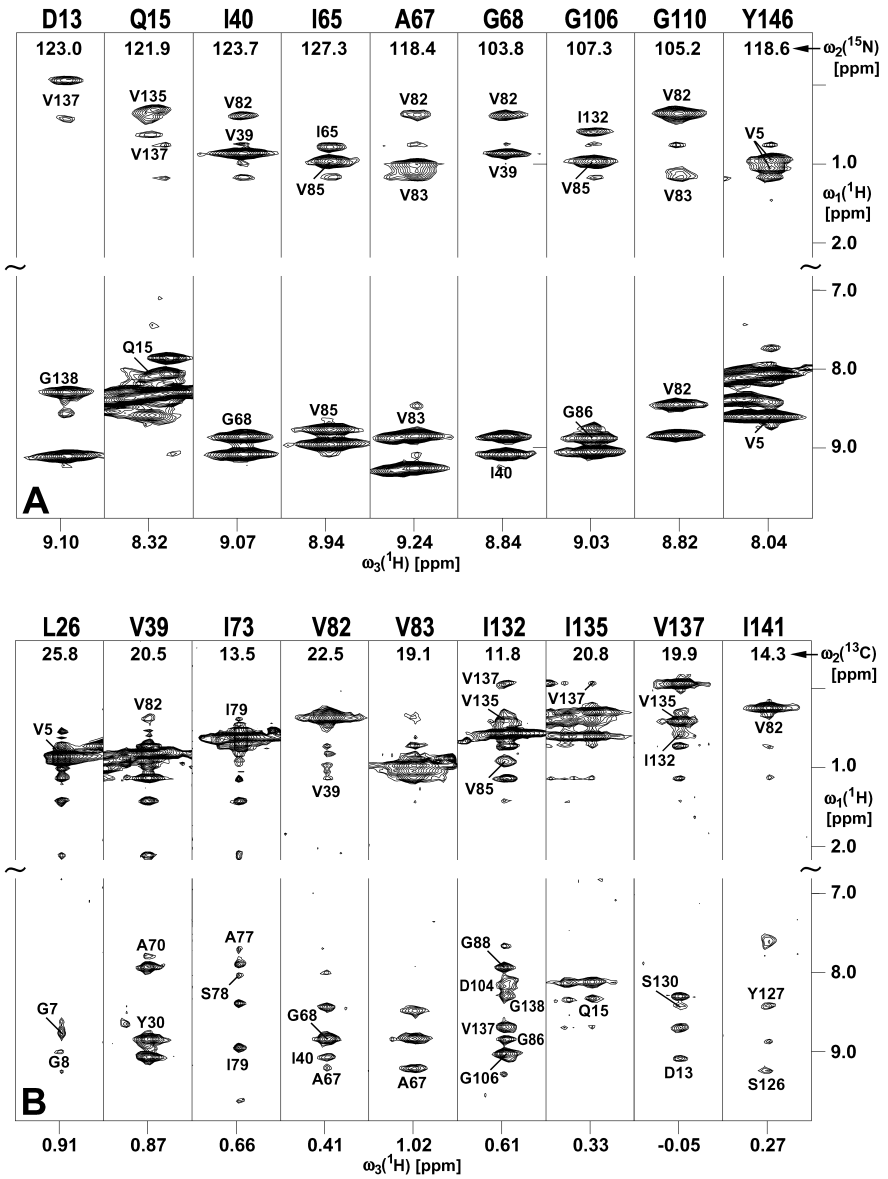

Figure 1. (A) 3D ^{15}N-resolved [^{1}H,^{1}H]-NOESY spectrum of OmpX/DHPC. (B) 3D ^{13}C-resolved [^{1}H,^{1}H]-NOESY spectrum. [$\omega_1(^1H)$,$\omega_3(^1H)$]-strips were taken at the ^{15}N or ^{13}C chemical shifts specified at the top and centered about the amide proton chemical shifts or the methyl proton chemical shifts, respectively, of the amino acid residues indicated. Cross-peaks indicating long-range and medium-range NOE connectivities are labeled with the one-letter amino acid symbol and the sequence number of the partner residue. The unlabeled peaks are either diagonal peaks, cross-peaks arising from intraresidual or sequential NOEs, or intermolecular NOEs to DHPC molecules.[25] The spectra were recorded with a 2 mM solution of [u-^{2}H,^{13}C,^{15}N/L,V,Iδ^{1}-$^{13}CH_3$]-OmpX/DHPC at 30 °C.

Leu, and Ile residues, which include both methyl–H^N and methyl–methyl NOEs, are located in the well-defined β-barrel region, which also has the majority of the long-range interstrand H^N–H^N NOEs (Figure 3(D)).

To further characterize the nature of the increased disorder in the loops and turns, we measured heteronuclear ^{15}N{^{1}H}-NOEs, which are sensitive to the mobility of individual N–H bonds on the picosecond to nanosecond time scale. The ^{15}N{^{1}H}-NOEs have significantly lower values for the residues located in and at the boundaries of the loops L1, T1, L2 and L3 (colored red in Figure 3(C)), indicating increased mobility of these polypeptide regions. Particularly low ^{15}N{^{1}H}-NOE values were observed for the loops L2 and L3, which also have the largest displacements (Figure 3(B)). These mobile regions include the residues located in the protruding parts of the strands β5 and β6, and the two residues closest to L2 in the strands β3 and β4. The ^{15}N{^{1}H}-NOE data thus indicate for these four polypeptide regions that dynamic processes are responsible for the comparatively poor definition of the structure. For the remaining loops T2, T3 and L4, the heteronuclear NOE data provide no evidence for fast

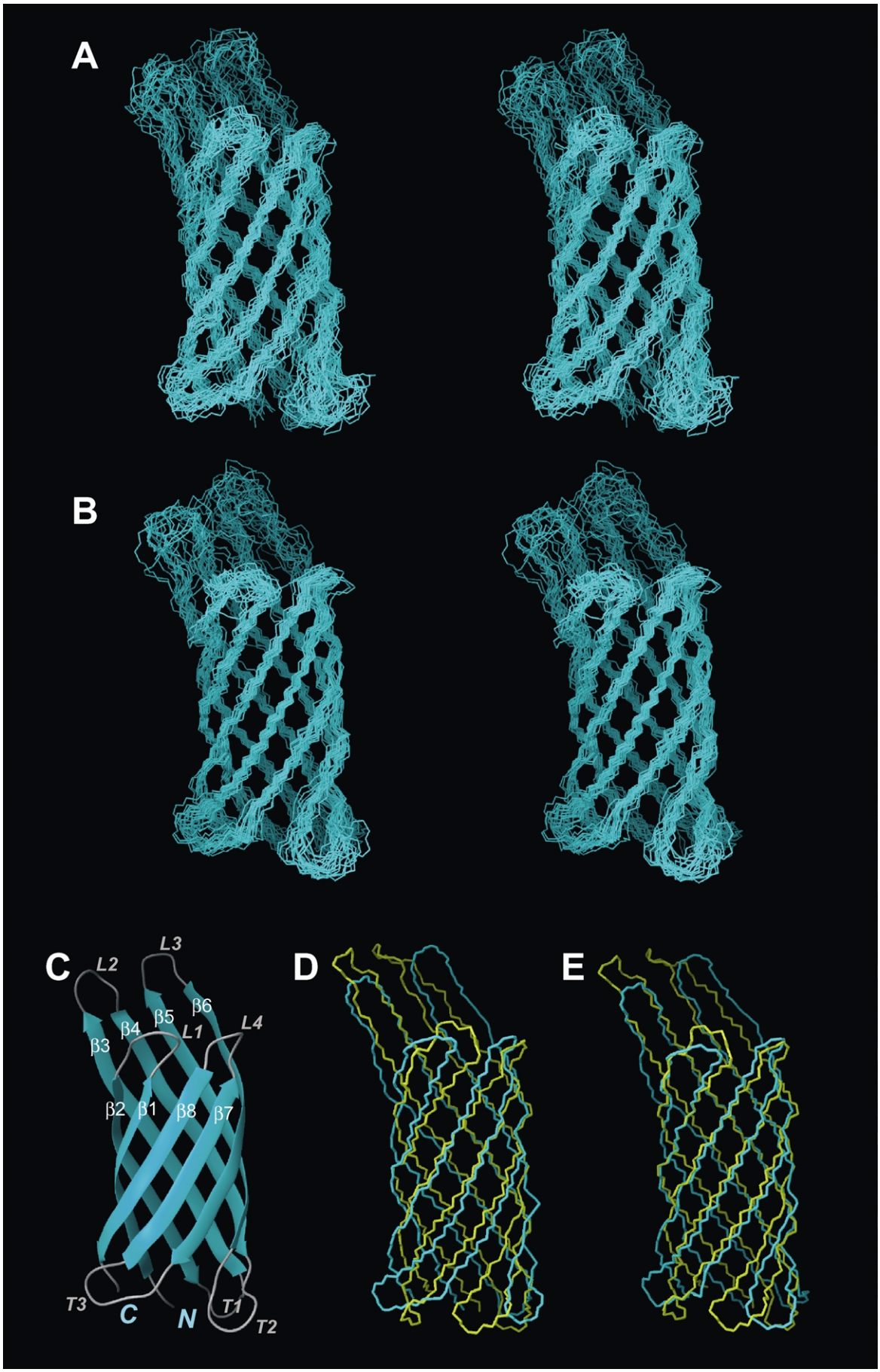

Figure 2 (*legend opposite*)

motional processes (Figure 3(C)). The reduced precision of the structure determination of these polypeptide segments thus seems to arise from scarcity of long-range NOE distance constraints (Figure 3(D)), which may in turn be related to slower dynamic processes on the millisecond to microsecond time scale.

Backbone amide proton exchange rates were determined from a series of 2D [^{15}N,^{1}H]-TROSY spectra recorded at variable time intervals after lyophilized H^N-protonated OmpX/DHPC had been dissolved in $^{2}H_2O$. Slowed exchange was observed for all amide groups involved in the hydrogen bonds identified in the regular secondary structures (Figures 3(D) and 4(B)) of the energy-minimized OmpX/DHPC structures. An exception is the amide protons in the protruding β-sheet, which show only weak protection from exchange and thus indicate local fraying of this part of the molecular structure. The ^{15}N{^{1}H}-NOE data (Figures 3(C) and 4(A)) then further indicate that fraying of the protruding β-sheet is a high-frequency process.

Discussion

Impact of selective Val, Leu, and Ile(δ^1) methyl group protonation

In OmpX/DHPC, specific ^{1}H-labeling, sequence-specific and stereospecific assignment of the Val, Leu, and Ile(δ^1) methyl groups[20,23] yielded a four-fold increase in the number of NOE distance constraints. The impact is such that we now have a good quality structure, whereas the previous studies, which were based exclusively on amide group protonation on a perdeuterated background, could only yield a low-precision, but nonetheless correct backbone fold.[10] The NOE data including only backbone H^N–H^N distance constraints yielded an RMSD value to the mean coordinates of 2.13 Å for the backbone atoms of the residues located in the regular secondary structure elements, whereas the corresponding number for the presently described structure is 1.42 Å (Table 1). The approach applied here can thus lead to a significant improvement of the NMR structures of proteins in large structures, where extensive deuteration is required for obtaining high-resolution NMR spectra. For α-helical membrane proteins it can be expected that NOEs involving methyl groups will be essential already for defining the global fold of the protein, i.e. the relative spatial locations of multiple helical secondary structures, and thus to open an avenue for *de novo* structure determination of this class of membrane proteins by NMR in solution.

Comparison of the NMR solution structure of OmpX with the X-ray crystal structure

The solution structure of OmpX/DHPC closely resembles the X-ray structure obtained in the presence of the detergent *n*-octyltetraoxyethylene.[18] The RMSD values relative to the X-ray crystal structure calculated for the backbone atoms located in the regular secondary structure elements are 2.29 Å for the mean NMR structure obtained from data set I (Figure 2(D)), and 1.92 Å for the NMR structures obtained from data set II (Figure 2(E)). The crystal and solution structures have the same overall dimensions and the same ellipsoidal cross-section measures, with a ratio of 1.6 between the longest and the shortest axis. In the NMR structure, the β-strands of OmpX are on average two residues shorter than in the crystal structure, which may in part be a consequence of the poorer definition of the loops due to the scarcity of long-range experimental constraints in these regions (Figure 3(D)). Both structures contain the protruding β-sheet at the extracellular end, which is clearly defined in solution by numerous interstrand NOEs (Figure 5). Overall, in the crystals as well as in solution, OmpX thus fits the folding rules[24] proposed for all β-barrels from bacterial outer membranes, with an even number of β-strands, the N and C termini at the periplasmic barrel end, and a central β-barrel surface of hydrophobic side-chains forming a non-polar ribbon lined by two girdles of aromatic side-chains.

The close similarity of the X-ray crystal and NMR solution structures of OmpX, which is quite remarkable taking into account the differences in the environments used to obtain the two structures, provides an opportunity for investigating complementary features of the data obtained by the two methods. These bear primarily on conformational equilibria and intramolecular rate processes in the OmpX structure in the detergent

Figure 2. Solution NMR structures of OmpX in DHPC micelles. (A) Stereoview of the 20 energy-refined CYANA conformers representing the solution structure of OmpX/DHPC calculated using NOE-derived distance constraints and chemical shift-derived torsion angle constraints (data set I). (B) Same as (A) calculated with the data used in (A) plus hydrogen bond constraints that were automatically determined in the structures shown in (A) (data set II; see the text for details). (C) Ribbon representation of the solution structure of OmpX/DHPC. Regular β-strands are blue and the remaining regions gray. The β-strands β1–β8, the extracellular loops L1–L4, the periplasmic turns T1–T3, and the N and C termini are labeled. (D) Comparison of the NMR solution structure of OmpX in DHPC micelles (blue) obtained from the data set I (mean atom coordinates from (A)) with the X-ray crystal structure obtained in the detergent *n*-octyltetraoxyethylene (yellow). (E) Same as (D) using the NMR structure of OmpX in DHPC micelles (blue) obtained from the data set II (mean atom coordinates from (B)). The Figures have been prepared with the program MOLMOL.[36]

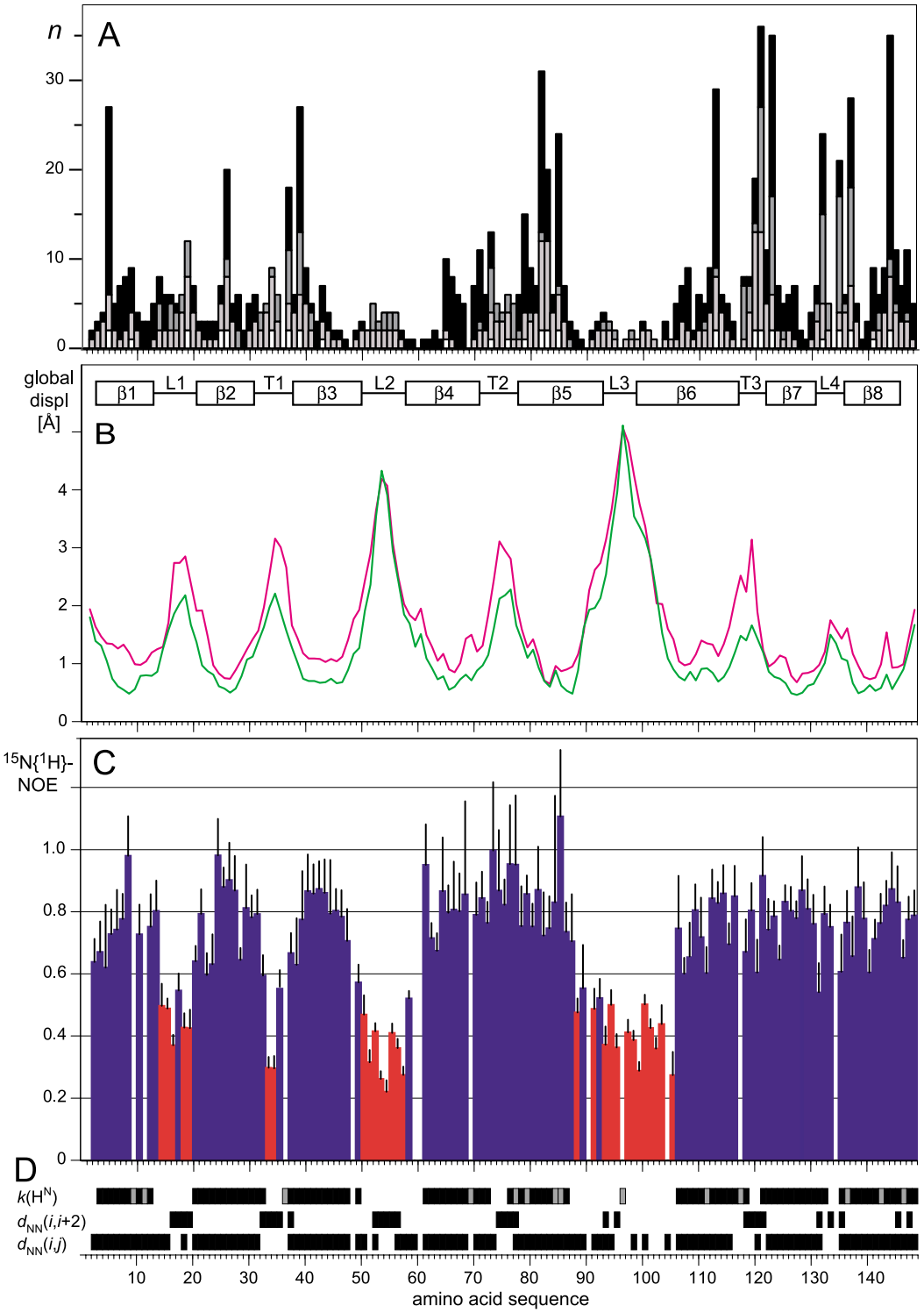

Figure 3. (A) Plot *versus* the amino acid sequence of the number of NOE constraints per residue, *n*, used in the calculation of the solution structure of OmpX/DHPC (white, intra-residual; light gray, short-range (difference in sequence position = 1); dark gray, medium-range (difference from 2 to 5); black, long-range (difference larger or equal 6)). (B) Plot *versus* the amino acid sequence of the global displacements[22] for the backbone atoms obtained with superposition of the backbone heavy atoms of the regular secondary structures (see Table 1) for minimal RMSD. The average over the 20 energy-refined CYANA conformers representing the NMR solution structure of OmpX/DHPC is shown. Magenta, structure calculated with the data set I; green, structure calculated with the data set II. The locations of the regular strands (β1–β8), the extracellular loops (L1–L4) and the periplasmic turns (T1–T3) are indicated at the top of (B). (C) Heteronuclear $^{15}N\{^1H\}$-NOEs of OmpX/DHPC measured at 500 MHz plotted *versus* the amino acid sequence. The positive half of the standard deviations is indicated by black vertical lines. Residues with heteronuclear $^{15}N\{^1H\}$-NOE values smaller than 0.5 are highlighted in red. (D) Amide proton exchange and $[^1H,^1H]$-NOE data. In the row $k(H^N)$, the residues with slowly exchanging amide protons ($k_{ex} < 0.2$ min^{-1}) are marked with black rectangles. Gray rectangles

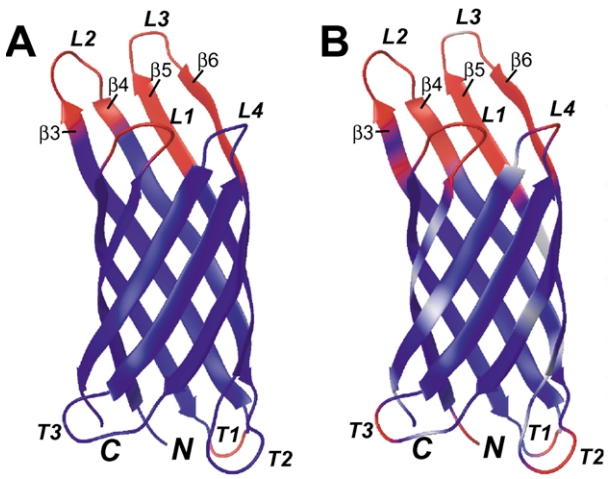

Figure 4. (A) Graphical representation of high frequency dynamic processes in OmpX/DHPC. Residues with backbone heteronuclear $^{15}N\{^1H\}$-NOE values smaller than 0.5 are colored red, those with values larger than 0.5 are blue. (B) Amide proton exchange rates. Residues colored in red did not show any detectable signal in a 2D [^{15}N,^1H]-TROSY spectrum recorded ten minutes after a lyophilized, protonated OmpX/DHPC sample was redissolved in ^2H_2O. Signals from the residues colored in blue were still detected after this time ($k_{ex} < 0.2\,min^{-1}$). For residues colored gray, the amide proton exchange rates could not be determined. The chain ends, the strands β3–β6, the extracellular loops and the periplasmic turns are identified.

Table 1. Experimental NMR data and structural statistics for OmpX

Quantity	No H-bond constraints (data set I)	H-bond constraints (data set II)
NOE upper distance limits		
Total	526	526
Long-range, spanning five or more residues	255	255
Constrained hydrogen bonds	–	34
Torsion angle constraints	172	172
Residual CYANA target function value, (Å^2)[a]	0.13 ± 0.06	0.25 ± 0.06
Distance constraint violation[a]		
Number >0.1 Å	5 ± 2	6 ± 2
Maximum (Å)	0.12 ± 0.01	0.12 ± 0.01
Torsion angle constraint violation[a]		
Number >2.5°	1 ± 1	1 ± 1
Maximum (deg.)	3.0 ± 0.5	3.1 ± 0.7
PROCHECK Ramachandran plot analysis[a]		
Residues in favored regions (%)	74 ± 3	74 ± 3
Residues in additional allowed regions (%)	21 ± 3	21 ± 3
Residues in generously allowed regions (%)	3 ± 2	3 ± 1
Residues in disallowed regions (%)	2 ± 1	2 ± 1
RMS distance to the averaged coordinates[a]		
N, C^α, C′ (best defined regions) (Å)[b]	1.13 ± 0.15	0.93 ± 0.13
N, C^α, C′ (regular β-structures) (Å)[c]	1.42 ± 0.16	1.17 ± 0.15
N, C^α, C′ (2–148) (Å)	1.90 ± 0.23	1.62 ± 0.24
All heavy atoms (2–148)	2.87 ± 0.21	2.52 ± 0.17

[a] The values given are the average and the standard deviation over the 20 energy-minimized conformers with the lowest residual CYANA target function values that represent the NMR solution structure.
[b] Includes the following 57 residues located in the center of the β-barrel: 6–10, 24–28, 41–47, 61–68, 81–90, 102–114, 125–128 and 139–143.
[c] Includes the following 105 residues located in the β-strands: 3–13, 21–31, 38–50, 58–71, 78–93, 99–117, 122–131 and 136–146.

environments, and on the extent to which the solvation of the protein by the detergent and the solvent water can be characterized.[25] Since these data bear quite directly on the functional interpretation of the OmpX structures, they are discussed in the following section.

Implications for the mode of action of OmpX in its physiological function

The *E. coli* outer membrane protein OmpX belongs to a family of highly conserved bacterial proteins that have been assigned key functions in promoting bacterial adhesion and entry into mammalian cells.[18] Based on the crystal structure of OmpX in the presence of the detergent *n*-octyltetraoxyethylene, it was postulated that the protruding β-sheet might present an epitope for binding of external proteins. Thereby, the edge of the β-sheet could act as a hydrogen bonding partner, and the resulting specific binding affinity has been suggested to play an important role in cell adhesion and invasion, and to cause virulence by interfering with the human complement defense system.[18] This interpretation of the OmpX crystal structure was hypothetical in the sense that the Asn residue in the sequence position 100 at the protruding extracellular end of the strand β6 (Figure 5) is involved in crystal contacts with a neighboring OmpX molecule. The OmpX solution structure now confirms the conclusion that the protruding β-sheet is a structural feature of native OmpX and not a crystal artifact. The protruding β-sheet seems to be a unique feature of OmpX,[18,24]

identify Pro residues or residues for which the amide proton exchange rates could not be measured due to spectral overlap or assignment ambiguity in the 2D [^{15}N,^1H]-TROSY spectra. The rows $d_{NN}(i,i+2)$ and $d_{NN}(i,j)$ with $|i-j| \geq 4$ indicate medium-range and long-range H^N–H^N NOE connectivities that were used as input for the structure calculation of OmpX/DHPC. Residues involved in such NOEs are indicated with black rectangles.

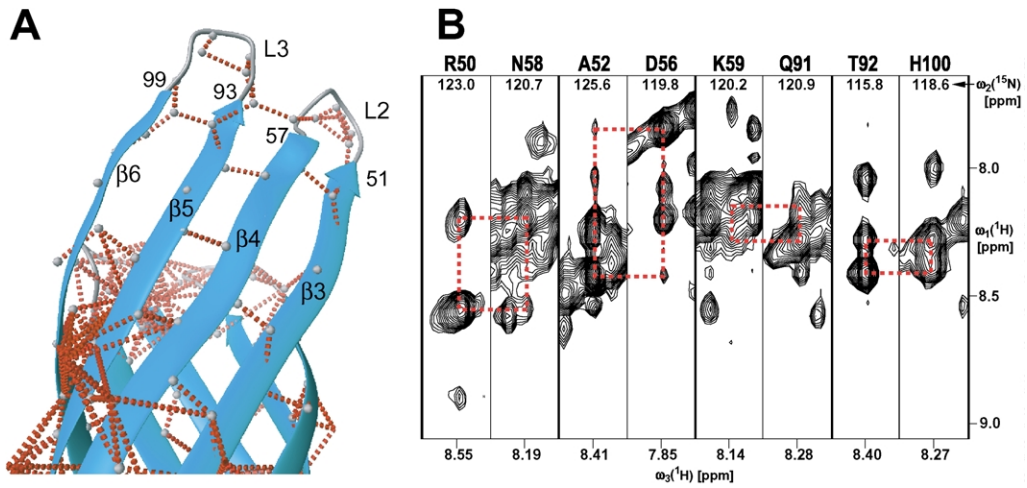

Figure 5. (A) Fragment of the OmpX/DHPC NMR structure comprising the extended, protruding β-sheet at the extracellular end of the strands β3, β4, β5 and β6. The NOE distance constraints used as input for the structure calculation are represented with red dotted lines. For improved clarity, the structure has been rotated by 180° about the long axis of the barrel with respect to the orientation shown in the previous illustrations. The loops L3 and L4, and the sequence positions of the extracellular ends of the strands β3–β6 are indicated. (B) [$\omega_1(^1H)$,$\omega_3(^1H)$]-strips from a 3D ^{15}N-resolved [^1H,^1H]-NOESY spectrum of OmpX/DHPC. The strips were taken at the amide ^{15}N chemical shifts specified at the top, $\omega_2(^{15}N)$, and centered about the amide proton chemical shifts, $\omega_3(^1H)$, of the amino acid residues indicated, which are all located in the molecular region shown in (A). Four of the interstrand NOEs represented in (A) are identified with red broken lines on the NMR spectrum.

since in all other known outer membrane protein structures this region contains long, structurally disordered loops with non-regular secondary structure. In particular, no evidence for the formation of a protruding β-sheet was seen in the NMR structures of the closely related protein OmpA either in DHPC[11] or in dodecylphosphocholine[12] micelles.

In view of its potential functional role, the protruding β-sheet in solution was further characterized with additional experimental data. In the solution structure of OmpX/DHPC, several long-range NOEs could be unambiguously identified between neighboring strands within the protruding β-sheet, particularly between residues R50 and N58, A52 and D56, Y57 and T93, K59 and Q91, Q61 and K89, G88 and D104, and T92 and H100 (Figure 5). Additional interstrand NOEs that one would expect from the thus clearly defined molecular structure may not have been detected due to exchange broadening, as suggested by the weak intensities of the cross-peaks for some residues of this molecular region in all measured spectra. Plasticity of the protruding β-sheet is implicated by the rapid exchange of the backbone amide protons ($k_{ex} > 0.2\ min^{-1}$) for the majority of the residues (Figure 4(B)). The observation of low heteronuclear NOE values ($^{15}N\{^1H\}$-NOE < 0.5) further shows that for the peripheral regions of the protruding β-sheet the transitions between hydrogen-bonded folded structure and solvent-exposed unfolded structure are mediated by high frequency processes (Figure 4(A)). It is of course tempting to speculate that the plasticity and the dynamics of this β-sheet are important features for optimal adaptation to the molecular targets, and help in finding the optimal orientation of this "waving flag" in recognizing its reaction partners.

There is pronounced complementarity of the X-ray and NMR data on the interactions with the detergents used for reconstituting the protein. In the crystal structure, only a single molecule of *n*-octyltetraoxyethylene could be located on the protein surface.[18] In contrast, in the mixed OmpX/DHPC micelles used to determine the OmpX solution structure, a large number of direct contacts between the hydrophobic tails of DHPC and the hydrophobic surface of the OmpX barrel were observed by NMR.[25] This study showed that the DHPC molecules are packed as a monolayer on the hydrophobic surface of the barrel, forming a cylinder jacket of about 28 Å in height located about the center of the barrel. Within the monolayer, the DHPC molecules undergo rapid lateral diffusion on the chemical shift time scale, i.e. in the millisecond to microsecond range. The micelle thus seems to mimic quite faithfully the embedding of the β-barrel in a double-layer lipid membrane. The best-defined regions of the solution structure of OmpX coincide with the cylinder jacket formed by the hydrophobic contact area of OmpX and DHPC,[25] suggesting that the lipid–protein interactions in OmpX/DHPC contribute to the stability of the β-barrel in the micelles. Since both ends of the barrel are freely accessible to the aqueous solvent, the OmpX/DHPC micelles should also be suitable for further studies of functional intermolecular interactions with OmpX.

Materials and Methods

Production of OmpX and NMR sample preparation

$^{2}H,^{13}C,^{15}N$-labeled OmpX was produced as described.[10] The preparation of selectively methyl-protonated and otherwise uniformly $^{2}H,^{13}C,^{15}N$-labeled OmpX, [u-$^{2}H,^{13}C,^{15}N$/L,V,Iδ^{1}-$^{13}CH_3$]-OmpX, was performed as reported.[20] A standard protocol for protein isolation, purification, refolding and reconstitution into detergent micelles was used.[10] The NMR sample conditions were: solvent H_2O; protein concentration, ~ 2 mM; buffer, 20 mM phosphate, 100 mM NaCl, 0.05% NaN_3, 200 mM DHPC, 5% $^{2}H_2O$, pH 6.5.

NMR experiments with OmpX/DHPC

All NMR experiments were measured at 30 °C. The TROSY triple resonance NMR experiments used for sequence-specific resonance assignment, as well as the ^{15}N-edited [$^{1}H,^{1}H$]-NOESY recorded with $^{2}H,^{13}C,^{15}N$-labeled OmpX have been described.[10] The sequence-specific and stereospecific assignment of the isopropyl methyl groups of Val, Leu, and Ile(δ^{1}) in [u-$^{2}H,^{13}C,^{15}N$/L,V,Iδ^{1}-$^{13}CH_3$]-OmpX/DHPC have also been described.[20,23]

The 3D ^{13}C- and ^{15}N-edited [$^{1}H,^{1}H$]-NOESY spectra used in this study were measured with a [u-$^{2}H,^{13}C,^{15}N$/L,V,Iδ^{1}-$^{13}CH_3$]-OmpX/DHPC sample on a Bruker DRX-800 spectrometer equipped with four radio-frequency channels for generating the ^{1}H, ^{2}H, ^{13}C and ^{15}N pulses, and a ^{1}H-{$^{13}C,^{15}N$}-triple resonance probe with an actively shielded z-gradient coil. The following parameters were used: 3D ^{15}N-resolved [$^{1}H,^{1}H$]-NOESY spectrum: time domain data size $150(t_1)\cdot40(t_2)\cdot1024(t_3)$ complex points, $t_{1max}(^{1}H) = 14.4$ ms, $t_{2max}(^{15}N) = 16.4$ ms, $t_{3max}(^{1}H^{N}) = 98.3$ ms, $\tau_m = 200$ ms; 3D ^{13}C-resolved [$^{1}H,^{1}H$]-NOESY spectrum: time domain data size $175(t_1)\cdot40(t_2)\cdot1024(t_3)$ complex points, $t_{1max}(^{1}H) = 18.2$ ms, $t_{2max}(^{13}C) = 9.9$ ms, $t_{3max}(^{1}H) = 106.5$ ms, $\tau_m = 200$ ms.

All spin relaxation measurements were recorded on a Bruker DRX-500 spectrometer equipped with four radio-frequency channels for generating the ^{1}H, ^{2}H, ^{13}C and ^{15}N pulses, and a ^{1}H-{$^{13}C,^{15}N$}-triple resonance cryoprobe with an actively shielded z-gradient coil. TROSY-based pulse sequences were used to obtain heteronuclear ^{15}N-{^{1}H}-NOEs.[26] The heteronuclear NOEs were calculated from two independently measured and integrated spectra as the ratio of peak volumes with and without ^{1}H-saturation. The errors were calculated from the standard deviations of the averaged values from the two data sets.

Amide proton exchange kinetics were measured from a series of 2D [$^{15}N,^{1}H$]-TROSY spectra at a proton frequency of 750 MHz, data size $170(t_1)\cdot2048(t_2)$ complex points, $t_{1max}(^{15}N) = 90$ ms, $t_{2max}(^{1}H) = 195$ ms. After dissolving lyophilized, protonated OmpX/DHPC in $^{2}H_2O$, such spectra were recorded in intervals of one hour over a period of 80 hours.

All spectra were Fourier transformed with the program PROSA[27] and analyzed with XEASY.[28] Chemical shifts were referenced to internal 2,2-dimethyl-2-silapentane-5-sulfonate sodium salt (DSS).[29]

Calculation of the three-dimensional structure

NOE cross-peaks were assigned in the aforementioned NOESY spectra by a combination of interactive procedures and the automated CANDID method,[30] resulting in a total number of 526 unambiguously assigned upper distance limits: 220 between amide protons, 36 between methyl groups, 259 between amide and methyl groups, and 11 between amide and aromatic protons.[10] In addition, 172 backbone torsion angle constraints (86 for ϕ and 86 for ψ) were derived from chemical shift values using the program TALOS.[31] Stereospecific assignments for nine out of the 13 Val and Leu isopropyl groups were determined by biosynthetic fractional ^{13}C-labeling.[23,32] On the basis of this input, two structure calculations were performed with the program CYANA.[21] The first one used only these input data (data set I). For the second calculation the input data were supplemented by distance constraints for 34 backbone–backbone hydrogen bonds that were identified automatically by the program CYANA (data set II; see below). CYANA calculations started from 400 conformers with random torsion angle values. For each of these conformers, 10,000 torsion angle dynamics steps were performed during the standard simulated annealing schedule,[21] and the 20 conformers with lowest final target function values were subjected to restrained energy minimization with respect to the AMBER force field[33] in a water shell of 8 Å minimal thickness, using the program OPALp.[34,35]

The identification of hydrogen bonds was based on the structure obtained with the data set I and was performed with an automatic algorithm implemented in CYANA, which does not make any assumptions about the secondary structure or the protein topology. This routine identifies all potential backbone acceptor–donor pairs that are less than 3.5 Å apart in ten or more of the 20 best conformers and are separated by three or more residues along the sequence. Hydrogen bond distance constraints are then generated for those hydrogen atoms that are involved in exactly one potential acceptor–donor pair. Two upper and two lower distance limits are imposed for each hydrogen bond in order to restrict the H^{N}–O distance to the range 1.8–2.0 Å and the N–O distance to 2.7–3.0 Å.

Protein Data Bank accession numbers

Coordinates have been deposited in the Protein Data Bank under accession code 1Q9F (with H-bond constraints; data set II) and 1Q9G (without H-bond constraints; data set I).

Acknowledgements

Financial support was obtained from the National Center for Competence in Research (NCCR) Structural Biology, the Komission für Technologie und Innovation (KTI, project 3392.1) and the Schweizerischer Nationalfonds (project 31-49047.96). We thank Mrs Isabelle Allen for the careful processing of the manuscript.

References

1. Berman, H. M., Westbrook, J., Feng, Z., Gilliland, G., Bhat, T. N., Weissig, H. *et al.* (2000). The Protein Data Bank. *Nucl. Acids Res.* **28**, 235–242.

2. Tate, C. G. (2001). Overexpression of mammalian integral membrane proteins for structural studies. *FEBS Letters*, **504**, 94–98.
3. Grisshammer, R. & Tate, C. G. (1995). Overexpression of integral membrane proteins for structural studies. *Quart. Rev. Biophys.* **28**, 315–422.
4. von Jagow, G. & Scägger, H. (1994). *A Practical Guide to Membrane Protein Purification*, Academic Press, New York.
5. Pervushin, K., Riek, R., Wider, G. & Wüthrich, K. (1997). Attenuated T_2 relaxation by mutual cancellation of dipole–dipole coupling and chemical shift anisotropy indicates an avenue to NMR structures of very large biological macromolecules in solution. *Proc. Natl Acad. Sci. USA*, **94**, 12366–12371.
6. Gardner, K. H. & Kay, L. E. (1998). The use of ^{2}H, ^{13}C, ^{15}N multidimensional NMR to study the structure and dynamics of proteins. *Annu. Rev. Biophys. Biomol. Struct.* **27**, 357–406.
7. Salzmann, M., Pervushin, K., Wider, G., Senn, H. & Wüthrich, K. (2000). NMR assignment and secondary structure determination of an octameric 110 kDa protein using TROSY in triple resonance experiments. *J. Am. Chem. Soc.* **122**, 7543–7548.
8. Fiaux, J., Bertelsen, E. B., Horwich, A. L. & Wüthrich, K. (2002). NMR analysis of a 900 K GroEL–GroES complex. *Nature*, **418**, 207–211.
9. Tugarinov, V., Muhandiram, R., Ayed, A. & Kay, L. E. (2002). Four-dimensional NMR spectroscopy of a 723-residue protein: chemical shift assignments and secondary structure of malate synthase G. *J. Am. Chem. Soc.* **124**, 10025–10035.
10. Fernández, C., Adeishvili, K. & Wüthrich, K. (2001). Transverse relaxation-optimized NMR spectroscopy with the outer membrane protein OmpX in dihexanoyl phosphatidylcholine micelles. *Proc. Natl Acad. Sci. USA*, **98**, 2358–2363.
11. Fernández, C., Hilty, C., Bonjour, S., Adeishvili, K., Pervushin, K. & Wüthrich, K. (2001). Solution NMR studies of the integral membrane proteins OmpX and OmpA from *Escherichia coli*. *FEBS Letters*, **504**, 173–178.
12. Arora, A., Abildgaard, F., Bushweller, J. H. & Tamm, L. K. (2001). Structure of outer membrane protein A transmembrane domain by NMR spectroscopy. *Nature Struct. Biol.* **8**, 334–338.
13. Arora, A. & Tamm, L. K. (2001). Biophysical approaches to membrane protein structure determination. *Curr. Opin. Struct. Biol.* **11**, 540–547.
14. Hwang, P. M., Choy, W., Lo, E. I., Chen, L., Forman-Kay, J. D., Raetz, C. R. H. *et al.* (2002). Solution structure and dynamics of the outer membrane enzyme PagP by NMR. *Proc. Natl Acad. Sci. USA*, **99**, 13560–13565.
15. Oxenoid, K., Sönnichsen, F. D. & Sanders, C. R. (2002). Topology and secondary structure of the N-terminal domain of diacylglycerol kinase. *Biochemistry*, **41**, 12876–12882.
16. Oxenoid, K., Sönnichsen, F. D. & Sanders, C. R. (2001). Conformationally specific misfolding of an integral membrane protein. *Biochemistry*, **40**, 5111–5118.
17. Klein-Seetharaman, J., Reeves, P. J., Loewen, M. C., Getmanova, E. V., Chung, L., Schwalbe, H. *et al.* (2002). Solution NMR spectroscopy of [α-^{15}N]lysine-labeled rhodopsin: The single peak observed in both conventional and TROSY-type HSQC spectra is ascribed to Lys-339 in the carboxyl-terminal peptide sequence. *Proc. Natl. Acad. Sci. USA*, **99**, 3452–3457.
18. Vogt, J. & Schulz, G. E. (1999). The structure of the outer membrane protein OmpX from *Escherichia coli* reveals possible mechanisms of virulence. *Struct. Fold. Des.* **7**, 1301–1309.
19. Goto, N. K., Gardner, K. H., Mueller, G. A., Willis, R. C. & Kay, L. E. (1999). A robust and cost-effective method for the production of Val, Leu, Ile (δ^1) methyl-protonated ^{15}N-, ^{13}C-, ^{2}H-labeled proteins. *J. Biomol. NMR*, **13**, 369–374.
20. Hilty, C., Fernández, C., Wider, G. & Wüthrich, K. (2002). Side chain NMR assignments in the membrane protein OmpX reconstituted in DHPC micelles. *J. Biomol. NMR*, **23**, 289–301.
21. Güntert, P., Mumenthaler, C. & Wüthrich, K. (1997). Torsion angle dynamics for NMR structure calculation with the new program DYANA. *J. Mol. Biol.* **273**, 283–298.
22. Billeter, M., Kline, A. D., Braun, W., Huber, R. & Wüthrich, K. (1989). Comparison of the high-resolution structures of the alpha-amylase inhibitor tendamistat determined by nuclear magnetic-resonance in solution and by X-ray-diffraction in single-crystals. *J. Mol. Biol.* **206**, 677–687.
23. Hilty, C., Wider, G., Fernández, C. & Wüthrich, K. (2003). Stereospecific assignments of the isopropyl methyl groups of the membrane protein OmpX in DHPC micelles. *J. Biomol. NMR*, **27**, 377–382.
24. Schulz, G. E. (2000). β-barrel membrane proteins. *Curr. Opin. Struct. Biol.* **10**, 443–447.
25. Fernández, C., Hilty, C., Wider, G. & Wüthrich, K. (2002). Lipid–protein interactions in DHPC micelles containing the integral membrane protein OmpX investigated by NMR. *Proc. Natl Acad. Sci. USA*, **99**, 13533–13537.
26. Zhu, G., Xia, Y. L., Nicholson, L. K. & Sze, K. H. (2000). Protein dynamics measurements by TROSY-based NMR experiments. *J. Magn. Reson.* **143**, 423–426.
27. Güntert, P., Dötsch, V., Wider, G. & Wüthrich, K. (1992). Processing of multidimensional NMR data with the new software PROSA. *J. Biomol. NMR*, **2**, 619–629.
28. Bartels, C., Xia, T. H., Billeter, M., Güntert, P. & Wüthrich, K. (1995). The program XEASY for computer-supported NMR spectral analysis of biological macromolecules. *J. Biomol. NMR*, **6**, 1–10.
29. Markley, J. L., Bax, A., Arata, Y., Hilbers, C. W., Kaptein, R., Sykes, B. D. *et al.* (1998). Recommendations for the presentation of NMR structures of proteins and nucleic acids—IUPAC-IUBMB-IUPAB Inter-Union Task Group on the Standardization of Data Bases of Protein and Nucleic Acid Structures Determined by NMR Spectroscopy. *J. Biomol. NMR*, **12**, 1–23.
30. Herrmann, T., Güntert, P. & Wüthrich, K. (2002). Protein NMR structure determination with automated NOE assignment using the new software CANDID and the torsion angle dynamics algorithm DYANA. *J. Mol. Biol.* **319**, 209–217.
31. Cornilescu, G., Delaglio, F. & Bax, A. (1999). Protein backbone angle restraints from searching a database for chemical shift and sequence homology. *J. Biomol. NMR*, **13**, 289–302.
32. Senn, H., Werner, B., Messerle, B. A., Weber, C., Traber, R. & Wüthrich, K. (1989). Stereospecific assignment of the methyl ^{1}H NMR lines of valine and leucine in polypeptides by non-random ^{13}C labelling. *FEBS Letters*, **249**, 113–118.
33. Cornell, W. D., Cieplak, P., Bayly, I., Gould, I. R.,

Merz, K. M., Ferguson, D. M. *et al.* (1995). A second generation force field for the simulation of proteins, nucleic acids, and organic molecules. *J. Am. Chem. Soc.* **117**, 5179–5197.
34. Koradi, R., Billeter, M. & Güntert, P. (2000). Point-centered domain decomposition for parallel molecular dynamics simulation. *Comput. Phys. Commun.* **124**, 139–147.
35. Luginbühl, P., Güntert, P., Billeter, M. & Wüthrich, K. (1996). The new program OPAL for molecular dynamics simulations and energy refinements of biological macromolecules. *J. Biomol. NMR*, **8**, 136–146.
36. Koradi, R., Billeter, M. & Wüthrich, K. (1996). MOLMOL: a program for display and analysis of macromolecular structures. *J. Mol. Graph.* **14**, 51–55.

Edited by M. F. Summers

(Received 25 July 2003; accepted 9 September 2003)